Pore properties of Orai1 calcium channel dimers and their activation by the STIM1 ER calcium sensor

Received for publication, April 11, 2018, and in revised form, May 31, 2018 Published, Papers in Press, June 28, 2018, DOI 10.1074/jbc.RA118.003424

Xiangyu Cai[‡], Robert M. Nwokonko[‡], Natalia A. Loktionova[‡], Raz Abdulqadir[‡], James H. Baraniak, Jr.[‡], Youjun Wang[§], Mohamed Trebak[‡], Yandong Zhou[‡1], and Donald L. Gill[‡2]

From the [‡]Department of Cellular and Molecular Physiology, Pennsylvania State University College of Medicine, Hershey, Pennsylvania 17033 and the [§]Beijing Key Laboratory of Gene Resources and Molecular Development College of Life Sciences, Beijing Normal University, Beijing 100875, China

Edited by Roger J. Colbran

Store-operated Ca^{2+} entry signals are mediated by plasma membrane Orai channels activated through intermembrane coupling with Ca^{2+}-sensing STIM proteins in the endoplasmic reticulum (ER). The nature of this elaborate Orai-gating mechanism has remained enigmatic. Based on the *Drosophila* Orai structure, mammalian Orai1 channels are hexamers comprising three dimeric subunit pairs. We utilized concatenated Orai1 dimers to probe the function of key domains within the channel pore and gating regions. The Orai1-E106Q selectivity-filter mutant, widely considered a dominant pore blocker, was surprisingly nondominant within concatenated heterodimers with Orai1-WT. The Orai1-E106Q/WT heterodimer formed STIM1-activated nonselective cation channels with significantly enlarged apparent pore diameter. Other Glu-106 substitutions entirely blocked the function of heterodimers with Orai1-WT. The hydrophobic pore-lining mutation V102C, which constitutively opens channels, was suppressed by Orai1-WT in the heterodimer. In contrast, the naturally occurring R91W pore-lining mutation associated with human immunodeficiency was completely dominant-negative over Orai-WT in heterodimers. Heterodimers containing the inhibitory K85E mutation extending outward from the pore helix gave an interesting partial effect on both channel activation and STIM1 binding, indicating an important allosteric link between the cytosolic Orai1 domains. The Orai1 C-terminal STIM1-binding domain mutation L273D powerfully blocked STIM1-induced channel activation. The Orai1-L273D/WT heterodimer had drastically impaired STIM1-induced channel gating but, unexpectedly, retained full STIM1 binding. This reveals the critical role of Leu-273 in transducing the STIM1-binding signal into the allosteric conformational change that initiates channel gating. Overall, our results provide important new insights into the role of key functional domains that mediate STIM1-induced gating of the Orai1 channel.

The ubiquitously expressed Orai channels are an evolutionarily conserved family of Ca^{2+} entry channels mediating "store-operated" Ca^{2+} signals. These signals play a crucial role in regulating key cellular responses, including gene expression, growth, secretion, and motility (1–4). Orai channels function in the plasma membrane (PM)[3] but are activated through a dynamic intermembrane coupling process between the ER and PM, mediated by STIM proteins. These ER membrane proteins are sensors of ER luminal Ca^{2+} changes and undergo an intricate unfolding process when Ca^{2+} stored in the ER becomes depleted (1–3, 5–7). The unfolded STIM1 protein extends from the ER membrane surface and becomes trapped in ER–PM junctions by attaching to the PM where it tethers and activates PM Orai1 channels (1, 2, 5–7). A considerable number of immunological, muscular, and inflammatory disease states are related to changes in the operation of STIM proteins and Orai channels (1, 8–10). Hence, our understanding of the molecular coupling and function of the two proteins has major translational significance. Although we have recently determined much on the function and organization of STIM and Orai proteins (11–14), there is still considerable uncertainty about how the proteins associate within junctions and how these interactions mediate opening of Orai channels and the generation of Ca^{2+} signals (1–4, 15, 16).

The highly Ca^{2+}-selective mammalian Orai1 channel bears close sequence homology with the *Drosophila* Orai (dOrai) channel from which the crystal structure was recently resolved (17). The dOrai channel protein has four transmembrane helices and is organized as a hexameric assembly of subunits (see Fig. 1*A*). Although earlier studies were interpreted to indicate a

This work was supported in whole or part by National Institutes of Health Grants R01 GM120783 and R01 GM109279 (to D. L. G.), National Institutes of Health Predoctoral Fellowship GM125376 (to R. M. N.), and a Penn State University Junior Faculty Development Program grant (to Y. Z.). The authors declare that they have no conflicts of interest with the contents of this article. The content is solely the responsibility of the authors and does not necessarily represent the official views of the National Institutes of Health.

This article was selected as one of our Editors' Picks.

This article contains Figs. S1–S6.

[1] To whom correspondence may be addressed: Dept. of Cellular and Molecular Physiology, Pennsylvania State University College of Medicine, 500 University Dr., Hershey, PA 17033. Tel.: 717-531-8567; Fax: 717-531-7667; E-mail: zhouyd@psu.edu.

[2] To whom correspondence may be addressed: Dept. of Cellular and Molecular Physiology, Pennsylvania State University College of Medicine, 500 University Dr., Hershey, PA 17033. Tel.: 717-531-8567; Fax: 717-531-7667; E-mail: dongill@psu.edu.

[3] The abbreviations used are: PM, plasma membrane; ER, endoplasmic reticulum; CRAC, Ca^{2+} release-activating Ca^{2+}; tdT, tdTomato; CFP, cyan fluorescent protein; BisTris, 2-[bis(2-hydroxyethyl)amino]-2-(hydroxymethyl)propane-1,3-diol; ECFP, enhanced CFP; YFP, yellow fluorescent protein; EYFP, enhanced YFP; HEDTA, *N*-(2-hydroxyethyl)ethylenediaminetriacetic acid; BAPTA, 1,2-bis(2-aminophenoxy)ethane-*N*,*N*,*N*′,*N*′-tetraacetic acid; TEA, tetraethylammonium; NMDG, *N*-methyl-D-glucamine.

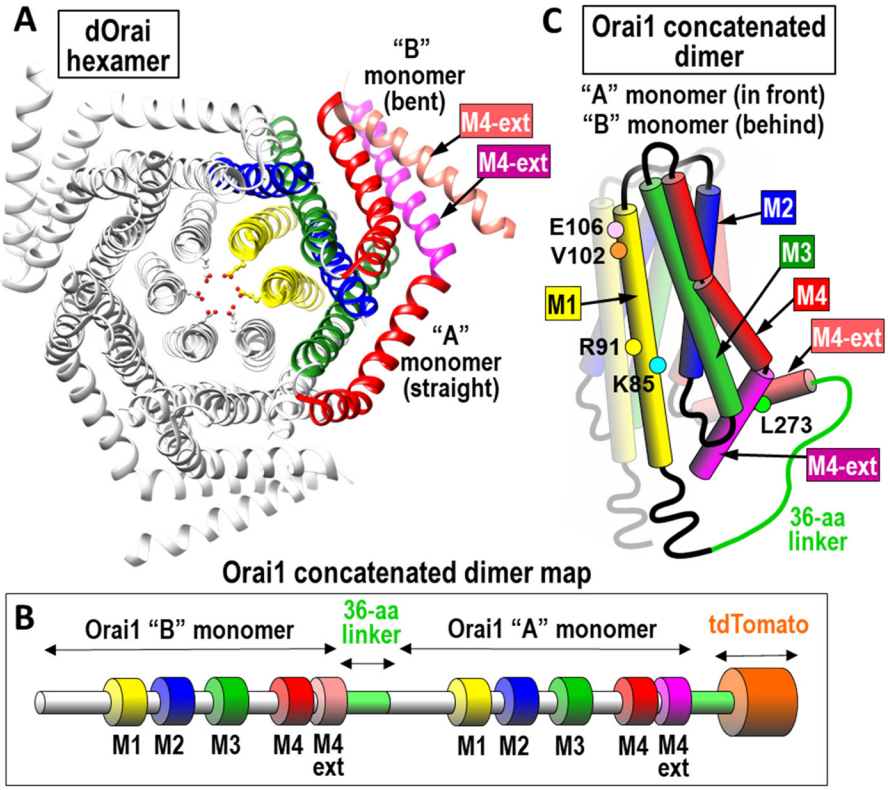

Figure 1. Structure of Orai channel and dimeric subunits. *A,* top view of *Drosophila* Orai channel hexamer. Two of the six monomers are colored to show one of the three dimers that constitute the channel. The two subunits in each dimer are almost identical except the "*A*" monomer has a straight M4 extension helix (M4-ext; *purple*) and the "*B*" monomer has a bent M4-ext (*pink*). The two M4-ext helices are linked in an antiparallel configuration by hydrophobic interactions. *B,* linear sequence of the concatenated Orai1 dimer constructs used; the two monomers are joined through a 36-amino acid linker sequence and tagged with tdTomato at the C terminus. Note: the sequences of the "*A*" and "*B*" monomers are the same. *C,* schematic of the concatenated Orai1 dimer structure. The membrane-spanning domains (M1, M2, M3, M4, and M4-ext) are labeled as shown. *Colored dots* reveal each of the point mutations used in this study.

tetrameric structure (18–24), recent evidence indicates the Orai1 channel functions as a hexamer (25, 26). Based on the dOrai crystal structure, most of the hexameric channel has 6-fold symmetry. The central pore is created from the six pore-forming N-terminal transmembrane helices (M1). Surrounding this are the tightly packed M2 and M3 helices, and at the periphery of the channel, the C-terminal M4 helices form STIM1-binding sites on the cytoplasmic face of the channel. The six M4 helices each have a small cytoplasmic extension (M4-ext; 39 amino acids in Orai1) that folds in two different configurations: one is almost straight from the M4-helix, and the other is bent almost 180° back on itself. Each adjacent pair of M4-ext helices closely interacts with one another in an antiparallel configuration. Thus, the STIM1-binding domain made up of the pair of M4-ext helices has 3-fold symmetry (see Fig. 1*A*). Unclear is whether these two M4-ext helices dissociate to form separate STIM1-binding sites (17, 27).

Because of the C-terminal interactions between adjacent pairs of M4-ext helices, the Orai channel comprises three dimers. Our studies therefore focused on the function of concatenated versions of these Orai1 dimers. Using such dimers, we were able to mutate either one or both of the separate Orai1 monomers, allowing us to gain important new information on the functional properties of the N-terminal pore–forming helix and the C-terminal STIM1–binding domain.

Results and discussion

Orai1 dimers, reliable probes for Orai1 structure/function

In a recent study, we compared the function of concatenated Orai1 channels of varying length (25). Surprisingly, we observed that concatemers containing 2–6 Orai1 subunits all give rise to authentic CRAC currents, similar to the expressed Orai1 monomer. Although Orai1 exists and functions as a hexamer, we concluded that the activity of concatemers containing 3–5 Orai1 subunits results from hexamers assembling from only the first two N-terminal subunits in the concatemer. This results in the formation of a hexameric "trimer of dimers," with the additional C-terminal Orai1 subunits in each concatemer (*i.e.* subunits beyond the initial N-terminal dimer) extending out from the hexamer and not contributing to function. The exceptions to this anomalous behavior were concatenated Orai1 dimers and hexamers. The hexamer appeared to largely form hexameric rings. The Orai1 dimers reliably assembled into hexameric Orai1 channels. We therefore constructed a series of Orai1 dimers (Fig. 1*B*) containing point mutations at functionally key residues, placed within either one or both subunits in the dimer (see Fig. 1*C*). For each construct, we assessed both the expression level (Fig. S1) and cellular location of expression (Fig. S2). In all cases, mutations did not alter either the level or the PM localization of Orai1 dimers. We expressed each mutant in HEK cells in which endogenous Orai1 was elim-

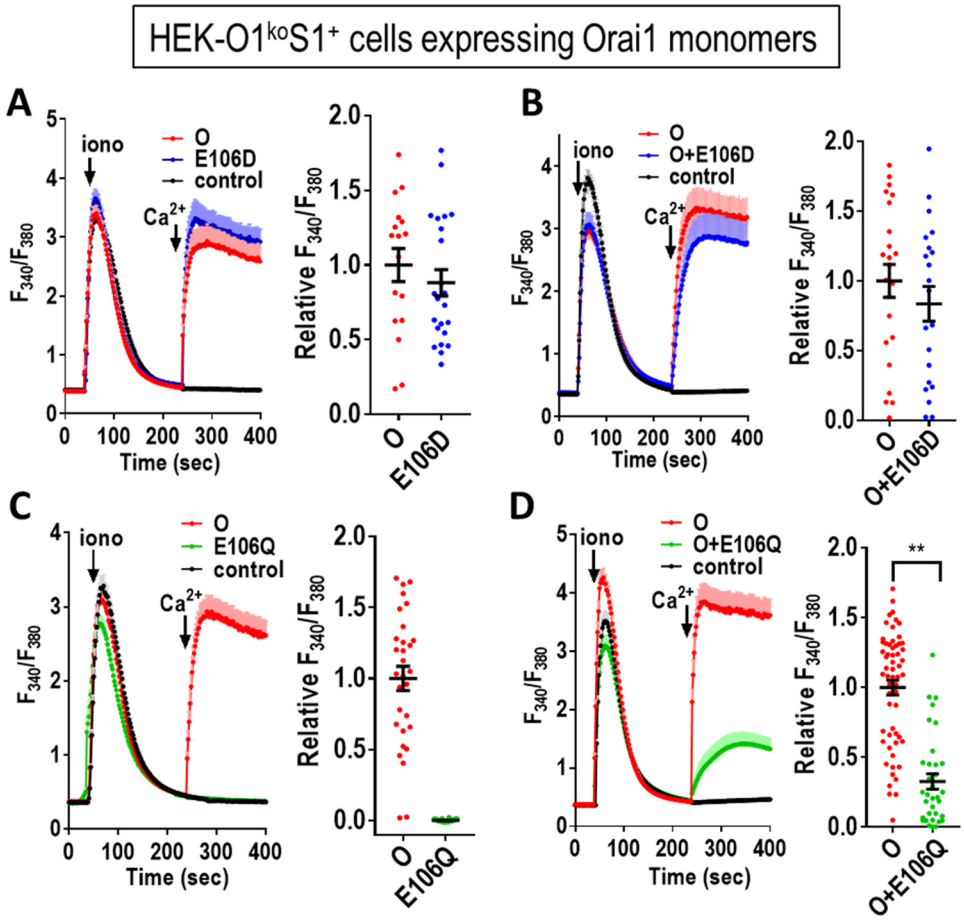

Figure 2. Consequences of mutating the selectivity filter (Glu-106) within expressed Orai1 monomers. tdTomato-tagged Orai1 monomer constructs were transiently expressed in HEK-O1^{ko}S1^{+} cells that stably express STIM1-YFP. Fura-2 ratiometric Ca^{2+} measurements were conducted to reveal cytosolic Ca^{2+} after store depletion with 2.5 μM ionomycin (*iono*) in Ca^{2+}-free medium followed by addition of 1 mM Ca^{2+} (*arrows*). *A,* cells were transfected with either Orai1-E106D (*E106D*) or Orai1-WT (*O*) or untransfected (*control*). *B,* cells were co-transfected with both Orai1-E106D-CFP and Orai1 WT or untransfected (*control*). *C,* cells were transfected with either Orai1-E106Q (*E106Q*) or Orai1-WT (*O*) or untransfected (*control*). *D,* cells were co-transfected with both Orai1-E106Q-CFP and Orai1-WT or untransfected (*control*). All the traces (means ± S.E.) are representative of three independent experiments. Summary scatter plots with means ± S.E. for normalized peak Ca^{2+} entry are for all individual cells recorded in three independent experiments. (**, $p < 0.005$).

inated through CRISPR/Cas9 gene editing, and STIM1-YFP was stably expressed (referred to as HEK-O1^{ko}S1^{+} cells) (25). The functional consequences of hetero- and homodimer mutations provided important new mechanistic information on Orai1 channel operation.

Dominance of selectivity filter mutations in Orai1 dimers

The Glu-106 residue is well established to function as the critical selectivity filter in the Orai1 channel (28–30). We initially examined the expression of Orai1 monomers containing the E106D and E106Q mutations, measuring their function either expressed alone or co-expressed with Orai1-WT (Fig. 2). The Orai1-E106D mutation has a shortened side chain that results in altered pore geometry and decreased channel selectivity (28–30). As expected, this mutation is still able to mediate Ca^{2+} entry (Fig. 2*A*), and co-expressed with Orai1-WT, the mutant has little effect (Fig. 2*B*). In contrast, removing the charge on the Glu-106 by replacing with Gln (but retaining side-chain length) gives a nonconducting pore (Fig. 2*C*). In this case, co-expression of Orai1-WT with Orai1-E106Q clearly causes inhibition of Ca^{2+} entry (Fig. 2*D*). This result was expected because the E106Q mutant has been recognized earlier as a "pore-dead" mutant (19, 29–32).

In such co-expression studies, the stoichiometry of subunits in hexamers is of course uncertain. Therefore, in further experiments, we compared the function of the E106D and E106Q subunits when incorporated into Orai1 dimer constructs. Initially, we combined Orai1-WT and Orai1-E106D subunits (Fig. 3, *A–C*). The Orai1-E106D homodimer (DD) gave rise to Ca^{2+} entry that was little different from the Orai1-WT homodimer, consistent with the data in Fig. 2 for monomer expression. The heterodimers of Orai1-WT and Orai1-E106D (OD and DO) also behaved similarly for Ca^{2+} entry. Using the Orai1-E106Q homodimer (QQ), there was no detectable Ca^{2+} entry (Fig. 3*D*), again consistent with the monomer in Fig. 2*C*. However, the heterodimers of Orai1-WT and Orai1-E106Q (OQ and QO) unexpectedly revealed strong Ca^{2+} entry, similar to that mediated by Orai1-WT (Fig. 3, *E* and *F*). This result is in stark contrast to heterodimers comprising Orai1-WT together with the Orai1-E106A mutant. For this mutant, the homodimer (AA) is clearly pore-dead (Fig. 3*G*), just like the Orai1-E106Q mutant (QQ). However, the heterodimers of Orai1-WT and Orai1-E106A (OA and AO) were also almost without function (Fig. 3, *H* and *I*).

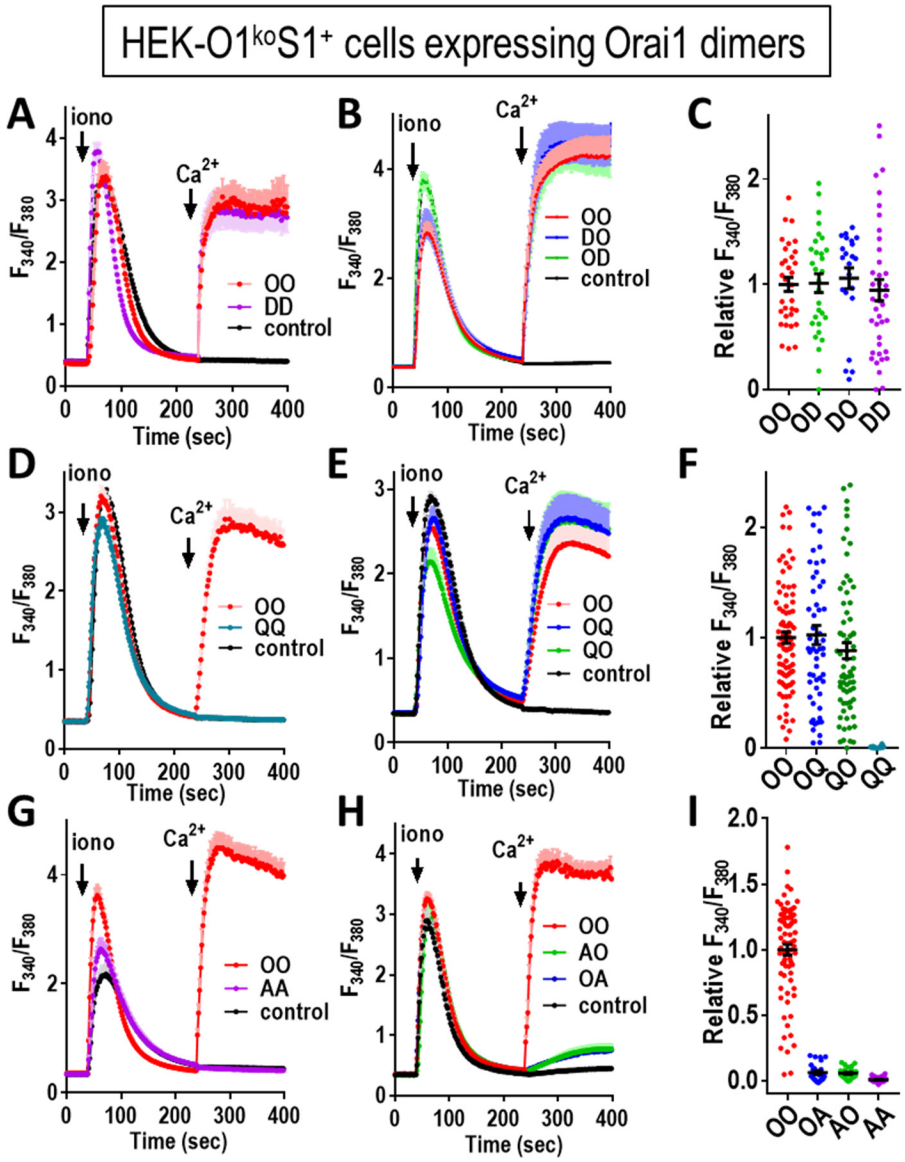

Figure 3. Function of concatenated Orai1 dimers containing the E106D and E106Q selectivity filter mutations. Orai1-tdT dimer constructs were transiently expressed at similar levels in HEK-O1^{ko}S1^{+} cells, and fura-2 ratiometric Ca^{2+} measurements were made to determine cytosolic Ca^{2+} after store depletion with 2.5 μM ionomycin (*iono*) in Ca^{2+}-free medium, followed by addition of 1 mM Ca^{2+} (*arrows*). *A,* cells were transfected with either Orai1-WT homodimer (*OO*) or Orai1-E106D homodimer (*DD*) or untransfected (*control*). *B,* cells were transfected with either OO or Orai1-WT/Orai1-E106D (*OD*), Orai1-E106D/Orai1-WT (*DO*), heterodimers, or untransfected (*control*). *C,* summary scatter plots with means ± S.E. for peak Ca^{2+} entry of all individual cells recorded in three independent experiments with the Orai1 concatemer constructs shown in *A* and *B*. *D,* cells were transfected with either Orai1-WT homodimer (*OO*) or Orai1-E106Q mutant homodimer (*QQ*) or were untransfected (*control*). *E,* cells were transfected with either OO or with Orai1-WT/Orai1-E106Q (*OQ*) or Orai1-E106Q/Orai1-WT (*QO*) dimer or were untransfected (*control*). *F,* summary scatter plots with means ± S.E. for peak Ca^{2+} entry of all individual cells recorded in three independent experiments with the Orai1 concatemer constructs shown in *D* and *E*. *G,* cells were transfected with either Orai1-WT dimer (*OO*) or Orai1-E106A homodimer (*AA*) or were untransfected (*control*). *H,* cells were transfected with either OO or Orai1-WT/Orai1E106A (*OA*) or Orai1-E106A/WT dimer (*AO*) or were untransfected (*control*). *I,* summary scatter plots with means ± S.E. for peak Ca^{2+} entry of all individual cells recorded in three independent experiments with the Orai1 concatemer constructs shown in (*G* and *H*). All the traces shown (means ± S.E.) are representative of three independent experiments.

This is important information because the action of E106Q has been widely described as both a pore-dead mutation and one that is dominant-negative over Orai1-WT subunits (1, 19, 29–32). Indeed, the dominance of E106Q has been described in Orai1 competition studies as providing evidence to support a purported tetrameric assembly of Orai1 channels (19). The dominance of E106Q was also the basis for its conditional transgenic expression in animal studies to assess the role of Orai1 in muscle tissue (33). Based on our studies here, although E106A and E106Q are clearly both pore-inactive mutations, their relative dominance in blocking Orai1-WT channels is very different. Clearly, such dominance studies would have been more conclusive using E106A instead of E106Q. The descriptions in earlier papers of the dominance of E106Q over Orai-WT (1, 19, 29–32) was in each case based on co-expression studies in which the relative expression of the Orai1 subunits could not be controlled. Only in concatemer studies can the ratio of expression be defined. Indeed, we used similar concatemeric constructs to reveal that E106L, E106V, E106G, and E106K all have complete dominance over Orai1-WT (Fig. S3).

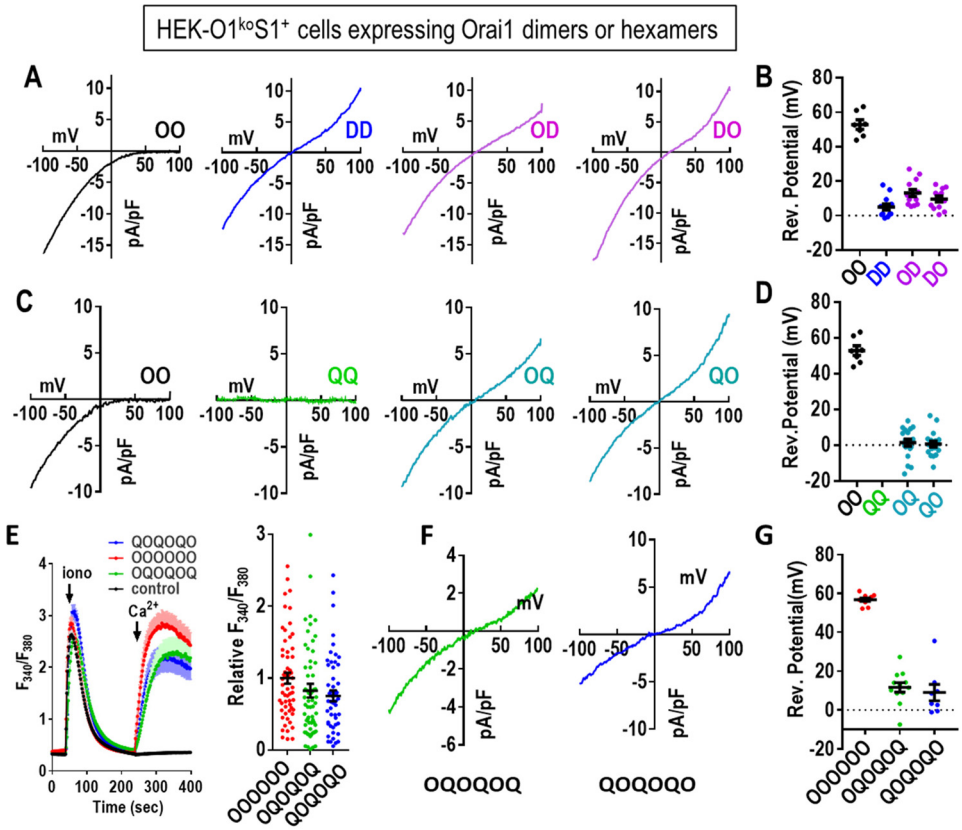

Figure 4. Electrophysiological properties of Orai1 E106D and E106Q concatenated dimers. *A,* representative *I/V* plots from whole-cell recordings using HEK-O1^{ko}S1^{+} cells transiently expressing each of the tdT-tagged concatenated Orai1 dimer constructs (OO, DD, OD, and DO) as described in Fig. 3. *B,* summary scatter plot (means ± S.E.) of reversal potential measurements taken from multiple *I/V* curves for the OO, DD, OD, and DO dimers shown in *A*. *C,* representative *I/V* plots from whole-cell recordings from HEK-O1^{ko}S1^{+} cells transiently expressing each of the tdT-tagged concatenated Orai1 dimer constructs (OO, QQ, OQ, and QO) as described in Fig. 3. *D,* summary scatter plot (means ± S.E.) of reversal potential measurements taken from multiple *I/V* curves for the QQ, OQ, and QO as shown in *C*. Current for the QQ construct was essentially zero. *E,* fura-2 ratiometric Ca^{2+} measurements reveal cytosolic Ca^{2+} after store depletion with 2.5 μM ionomycin (*iono*) in Ca^{2+}-free medium followed by addition of 1 mM Ca^{2+} (*arrows*). In each case, traces for Orai1-WT hexamer (*OOOOOO*) were compared with traces for Orai1 heterohexamers (*OQOQOQ* and *QOQOQO*). Untransfected control cells are also shown. *Traces* shown (means ± S.E.) are representative of three independent experiments. Summary scatter plots with means ± S.E. for peak Ca^{2+} entry of all individual cells recorded in three independent experiments with the Orai1 concatemer constructs shown. *F,* representative *I/V* relationship for the OQOQOQ and QOQOQO hexamers are shown. *G,* summary scatter plot (means ± S.E.) of reversal potential measurements taken from multiple *I/V* curves for the OOOOOO, OQOQOQ, and QOQOQO hexamers as shown in *F*.

Probing the anomalous functional characteristics of E106Q

The unexpected finding that OQ and QO heterodimers are functional prompted us to undertake an electrophysiological characterization to assess their selectivity and conductance. It was important to compare their function with constructs containing E106D because this mutation is known to convert the highly Ca^{2+}-selective Orai1 channel into a nonselective cation channel (28–30). As expected, the Orai1-WT homodimer (OO) gave typical CRAC current with full inward rectification and a reversal potential slightly above 50 mV (Fig. 4, *A* and *B*). In contrast, the Orai1-E106D homodimer (DD) gave rise to a nonselective current with a strong outward component and much reduced reversal potential (~5 mV; Fig. 4*B*). The reduction of a single methylene group by replacing the WT Glu-106 residue with Asp is reported to cause widening of the pore sufficient to make it cation-nonselective (34). Surprisingly, the presence of just a single aspartate in the E106D heterodimers (OD, DO) gave an *I/V* curve very similar to DD, with reversal potentials of ~10 mV (Fig. 4*B*). We would have expected that the properties of the heterodimeric channels (OD and DO) would be somewhere between the two homodimers. Thus, our results indicate that replacement of just three Glu residues with Asp in the selectivity filter of the hexameric channel is still sufficient to render it a nonselective channel.

The effects of the E106Q mutation are also surprising (Fig. 4, *C* and *D*). Clearly, the homodimeric replacement in QQ results in a channel with no conductance, as expected. However, the large but nonselective current seen with both the OQ and QO heterodimers was unexpected. In both cases, the reversal potential was close to 0 mV. Assuming the channel operates as a hexamer, this reveals that the full configuration of six charges in the selectivity filter is not required for cation conductance. Thus, the presence of just three negative charges in the pore filter is sufficient for strong cation permeation, albeit nonselectively.

We also examined the function of a concatenated hexameric Orai1 construct containing three pairs of OQ or QO dimers (Fig. 4, *E–G*). The function of both of these two hexamers was very comparable with that of their respective contributing heterodimers. For Ca^{2+} entry, both the OQOQOQ and QOQOQO hexamers gave similar function as the WT homohexamer (OOOOOO) (Fig. 4*E*). Current measurements with the hexamers revealed that both heterohexamers behaved as nonselective cation channels, similar to heterodimers. Reversal

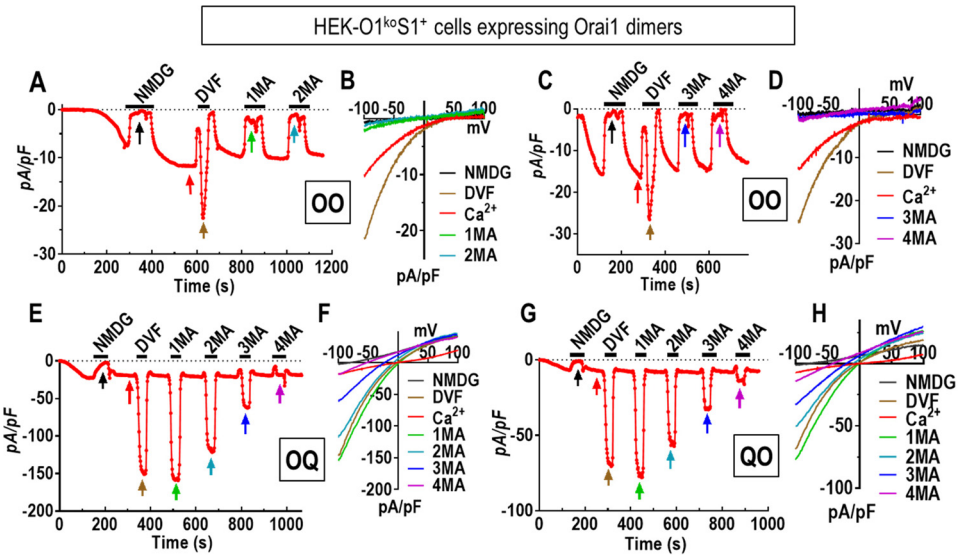

Figure 5. Altered pore properties of the nonselective Orai1 concatenated channel dimers OQ and QO. *A–D,* electrophysiological measurements using HEK-O1^{ko}S1^{+} cells expressing the Orai1-WT dimer (*OO*). Current developed initially in the presence of 20 mM Ca^{2+} in the external solution. Thereafter, the external solution was periodically switched from 20 mM Ca^{2+} with 130 mM Na^{+} to divalent cation-free solutions containing the following: 150 mM *N*-methyl-D-glucamine (NMDG), 150 mM Na^{+} (*DVF*), 150 mM methylammonium (*1MA*); 150 mM dimethylammonium (*2MA*); 150 mM trimethylammonium (*3MA*); and finally 150 mM tetramethylammonium (*4MA*). Between each divalent-free addition, cells were switched back to 20 mM Ca^{2+} with 130 mM Na^{+}. Current at −100 mV was plotted against time, and *I/V* relationships are shown (*B* and *D*) at the times indicated by *arrows* in *A* and *C*. *E,* using HEK-O1^{ko}S1^{+} cells expressing the OQ dimer, current developed in 20 mM external Ca^{2+}. After switching to NMDG, divalent solutions were again added in the external solution as shown in *A* and *C*. For channel formed by OQ heterodimers, methylated ammonium cation still can produce significant currents. *F, I/V* relationship of currents mediated by OQ collected in different external solutions as indicated by the *arrows* in *E*. *G,* HEK-O1^{ko}S1^{+} cells expressing the QO dimer were exposed to external solutions as shown in *E*. *H, I/V* relationship of currents mediated by QO collected in the external solutions indicated in *G*.

potential for hexamers was slightly elevated (Fig. 4*G*), and currents mediated by the hexamers were slightly smaller, perhaps due to less efficient expression compared with dimers. The similar function of both hexamers and dimers supports the view that the Orai1 channel is hexameric and comprises three pairs of dimers. In our previous paper (25), we concluded that a hexamer–concatemer could create a functional channel either as a single hexameric ring or as a trimer of dimers in which three concatemeric hexamers each contribute one dimer to form a single functional hexamer. The results we show here for the two heterohexamers would be consistent with either scheme.

Pore properties of the nonselective OQ and QO concatemer dimers

The surprising effect of replacing three glutamate residues with glutamines in the Orai1 selectivity filter prompted us to investigate whether this altered the channel pore diameter. For this, we measured the permeation of methylated ammonium derivatives of increasing size. We compared permeation of the OQ or QO Orai1 heterodimers with that of the OO WT homodimer expressed in HEK-O1^{ko}S1^{+} cells (Fig. 5). Consistent with previous studies expressing WT monomeric Orai1 (34, 35), we observed that the OO dimer had almost no current after switching from 20 mM Ca^{2+} to 150 mM methylammonium (Fig. 5, *A* and *B*). Increasing the methyl groups on methylammonium to two, three, and four, also revealed no measurable currents (Fig. 5, *C* and *D*). These results are similar to earlier results from which the Orai1 pore size was calculated to be ~3.9 Å (34, 35). In contrast, using cells expressing the OQ heterodimer, switching from Ca^{2+} to methylammonium resulted in a massive increase in current (Fig. 5, *E* and *F*). Moreover, large currents were still observed following consecutive switching from Ca^{2+} to dimethylammonium or even trimethylammonium. The same current measurements using the QO construct provided very similar results (Fig. 5, *G* and *H*). In both cases, the decreased currents and increasingly negative reversal potentials seen with increasing the number of methyl groups on ammonium ion allowed us to estimate an apparent pore diameter for the OQ and QO constructs considerably greater than the WT pore (see "Experimental procedures" and Fig. S4; this estimate is based on the assumption that permeability is limited only by the steric properties of the pore). We also constructed equivalent Orai1 heterodimers containing Glu-106 residues mutated to asparagine instead of glutamine (ON, NO, and NN). Ca^{2+} measurements revealed a similar functional pattern; NN gave no Ca^{2+} entry, whereas ON and NO gave Ca^{2+} entry identical to the WT OO (Fig. S5, *A* and *B*). Current measurements revealed the ON and NO dimers had similar ion nonselectivity (Fig. S5, *C–E*), and currents measured with methylated ammonium ions (Fig. S5, *F–M*) indicated similarly enlarged estimated pore size.

These surprising results clearly reveal that reducing the number of negatively charged residues in the selectivity filter of Orai1 from six (in the WT hexamer formed from OO) to three (formed by the OQ, QO, ON, or NO dimers) causes a substantial increase in apparent pore diameter and a major alteration in ion channel selectivity. This change in pore properties was even larger than that resulting from substitution of all six Glu-106 residues within the hexamer with Asp residues, indicating that both charge density and steric influence of headgroup size contribute to the geometry of the pore. The results with the OQ and ON heterodimers also gives support to a recent hypothesis on

the ion-selectivity mechanism for the Orai channel. Thus, in an interesting new crystallography study on dOrai channel structure, Hou *et al.* (36) suggest that glutamates comprising the selectivity filter have side-chain flexibility that allows two Ca^{2+} ions to be positioned one above the other. Repulsion between the two Ca^{2+} ions allows one Ca^{2+} to be displaced and move through the pore and to be replaced by a new Ca^{2+} ion. Thus in the presence of external Ca^{2+}, the channel is highly Ca^{2+}-selective. In the case that three glutamates are replaced with three similarly sized but uncharged glutamines, we would suggest that the selectivity filter loses the ability to bind two Ca^{2+} ions; Ca^{2+} selectivity would be lost, and monovalent cations would permeate in the presence of external Ca^{2+}.

Orai1 dimers mutated elsewhere in the Orai1 M1 pore-forming helix

In further experiments, we assessed the role of substituting other pore-lining residues within the Orai1 heterodimers. Immediately below the Glu-106 selectivity filter, the hexameric pore is lined with three rings of hydrophobic residues, thought to act as a hydrophobic gate (37). Mutating the first of these residues (*V102,* see Fig. 1*C*) to Cys causes the channel to be constitutively active, although with altered cation selectivity (37). Using an Orai1 V102C homodimer (CC), we observed substantial constitutive Ca^{2+} entry in HEK-O1^{ko} cells (not overexpressing STIM1) (Fig. 6*A* and Fig. S6*A*). Patch-clamp measurements also revealed a substantial current (Fig. 6*B* and Fig. S6*B*) with a reversal potential of approximately +25 mV (Fig. 6*C* and Fig. S6*C*). These results all agree closely with studies expressing monomer Orai1-V102C (13, 37). In contrast, the heterodimers containing one Orai1-WT and one Orai1-V102C subunit (OC or CO) displayed no constitutive Ca^{2+} entry or current (Fig. 6, *A–C*). Using HEK-O1^{ko}S1^{+}, we measured currents after depletion of stores following break-in with 20 mM BAPTA in the pipette. Cells expressing the CC homodimer revealed a typical CRAC-like store-dependent current with reversal potential greater than +50 mV (Fig. 6*D* and Fig. S6*D*), in close agreement with the earlier results with the Orai1-V102C monomer (13, 37). In similar experiments, the two Orai1 heterodimers, OC and CO, gave current properties almost identical to those seen with CC. The results are interesting in revealing that the WT Val at position 102 is dominant over the Cys mutant in the heterodimer. We might have expected that the heterodimer would have some constitutive function, but instead the hydrophobic gating function of this residue appears to be maintained with just three hydrophobic Val residues lining the pore. Conversely, the constitutive activation of Ca^{2+} entry by V102C appears to require mutation of all six residues.

This result is an interesting contrast to experiments to assess the function of a different pore-lining residue, Arg-91, residing below the hydrophobic pore region (Fig. 1*C*). The Arg-91 residue lies within the highly positively charged region of the pore toward the cytosolic side of the channel. The naturally occurring R91W mutation has been reported to cause severe combined immunodeficiency in homozygous patients (28). We constructed Orai1 mutant heterodimers with one R91W mutation (OW and WO). Expressed in HEK-O1^{ko}S1^{+} cells, we observed that the Orai1 heterodimers, OW and WO, each gave no store-dependent Ca^{2+} entry (Fig. 6, *E* and *F*). Indeed, their action was virtually the same as nontransfected cells. This result is quite different from that reported earlier (38) in which co-expression of Orai1-WT and Orai1-R91W resulted in only a modest slowing of the activation of I_{CRAC}. In that study, it is likely that the expression of WT and mutant R91W was not equal, in contrast to the OW and WO heterodimers. Another earlier study examined tetramer-concatemers of Orai1 in which 1, 2, 3, or all 4 WT Orai1 subunits were substituted with Orai1-R91W subunits (39). In that study, a single R91W residue caused 50% loss of activity, and with 2 or 3 mutant subunits, there was almost 100% loss of activity. Our results would concur with this dominance observed with R91W. However, the use of the tetrameric construct is difficult to reconcile because the Orai1 channel functions as a hexamer (17, 25, 26). Most likely, the expressed tetramers form hexamers through trimers of dimers, as described above. Given the almost complete dominance of the R91W in our heterodimers, patients heterozygous for the R91W gene would be expected to have substantially reduced Orai1-mediated Ca^{2+} entry. Such heterozygous R91W carriers had T cells with ~50% of WT Ca^{2+} entry (28). It is possible that compensatory expression of other Orai subtypes may have occurred in such patients.

We next used Orai1 dimers to examine the effects of mutating one of the residues of the pore-forming M1 helix that is not lining the pore (see Fig. 1*C*). The Lys-85 residue has been the center of much attention because the K85E mutation completely blocks store-dependent channel activation (13, 40–42). This residue faces outward from the pore-forming helix with its headgroup likely extending into the cytosol close to the cytosolic membrane surface. Using Orai1 homodimers with both Lys-85 residues mutated to Glu, we determined that there was no Ca^{2+} entry function, consistent with the blocking action determined earlier (Fig. 6, *G* and *I*) (40). Interestingly, we observed that the heterodimers with a single K85E mutation (OE and EO), each displayed a Ca^{2+} entry that was ~50% of the OO-WT homodimer (Fig. 6*H*). Current analysis confirmed that OE and EO had similarly diminished channel function and that the *I*/*V* relationship revealed each mediated otherwise normal CRAC current (Fig. 6, *J* and *K*, and Fig. S6*E*). Because the Lys-85 site has been implicated in binding STIM1 to possibly gate the channel (40–42), we also examined FRET between CFP-tagged Orai1 dimers (C-terminally labeled) and STIM1-YFP. In these studies, we observed FRET with each heterodimer (OE or EO) was decreased ~30% compared with the WT homodimer (Fig. 6*L*). The EE mutant homodimer gave a slight further decrease in FRET.

The K85E mutation has been the subject of considerable speculation. It clearly has a profound effect on the store-operated activation of Orai1 channels. It was speculated that Lys-85 mediates gating through possible interactions of STIM1 with the cytosolically-protruding extension of the pore-forming M1 helix (M1-ext) (40–42). However, recent studies suggest that Lys-85 is necessary for maintaining the configuration of the channel rather than directly mediating channel gating (13). Nevertheless, our current results do show that altering the cytosolic M1 extension (K85E) does affect binding of STIM1.

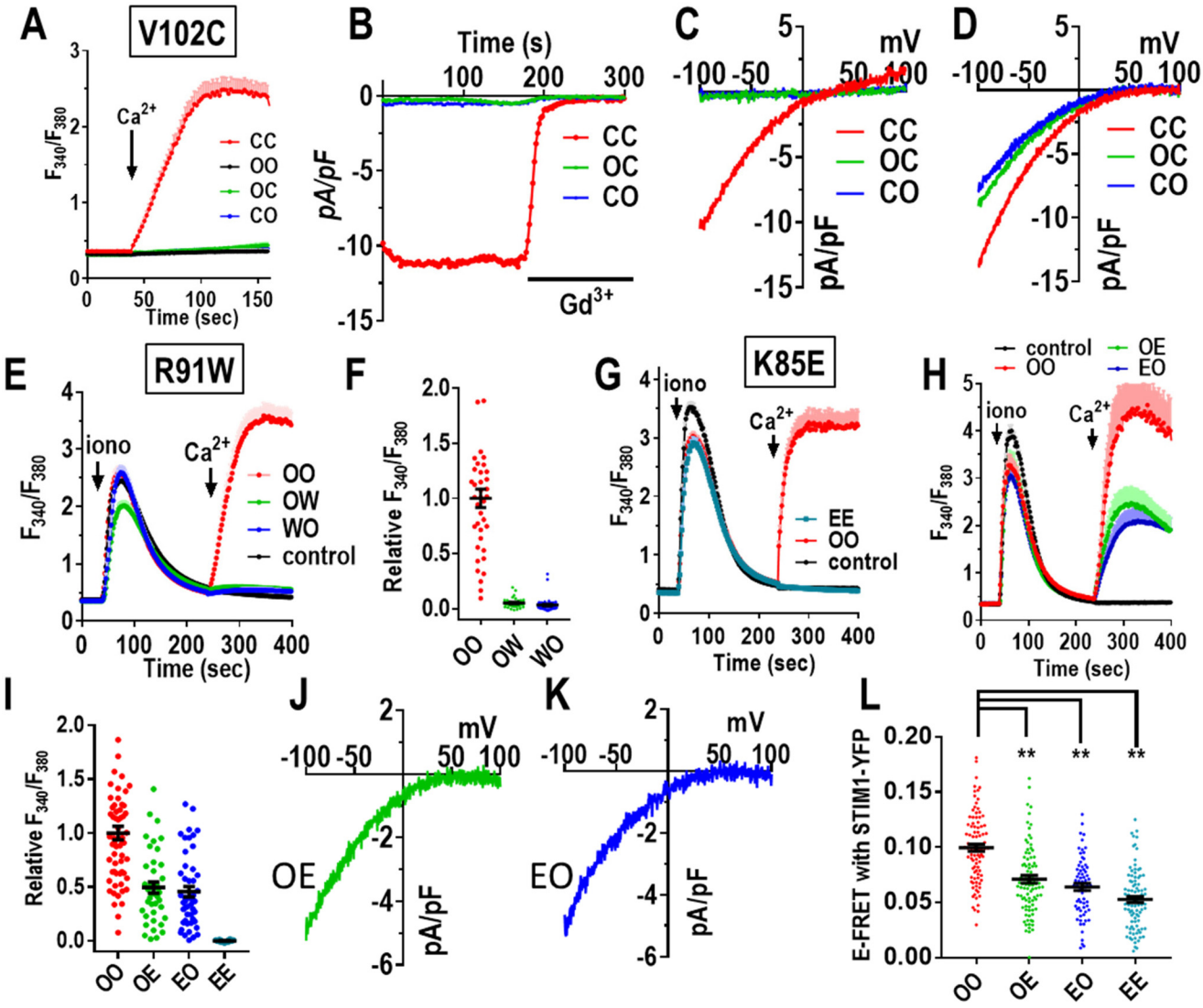

Figure 6. Mutation of key Orai1 channel pore residues in concatenated dimers. *A,* fura-2 ratiometric Ca^{2+} add-back measurements for HEK-O1^{ko} cells expressing similar levels of the C-terminal tdT-tagged Orai1 dimers OO (Orai1-WT/Orai1-WT), OC (Orai1-WT/Orai1-V102C), (Orai1-V102C/ Orai1-WT), or CC (Orai1-V102C/Orai1-V102C). Constitutive Ca^{2+} entry was measured after addition of 1 mM Ca^{2+} (*arrows*) after Ca^{2+}-free medium. *Traces* (means ± S.E.) are representative of three independent experiments. *B,* whole-cell patch–clamp recording of HEK-O1^{ko} cells expressing CC, OC, or CO; current at −100 mV was plotted against time. Cytosolic Ca^{2+} was maintained at 90 nM with BAPTA to prevent store depletion. Constitutive current was measured in 20 mM Ca^{2+} external solution, followed by blockade with 10 μM Gd^{3+}. *C,* representative *I/V* curves for the constitutive currents of the HEK-O1^{ko} cells expressing OC, CO, and CC shown in *B*. *D,* representative *I/V* curves for Ca^{2+} currents following store depletion with 20 mM BAPTA in HEK-O1^{ko}S1^{+} cells transiently expressing OC, CO, and CC. *E,* Ca^{2+} add-back measurements in fura-2–loaded HEK-O1^{ko}S1^{+} cells expressing similar levels of the C-terminal tdT-tagged Orai1 dimers OO (Orai1-WT/Orai1-WT), OW (Orai1-WT/Orai1-R91W), or WO (Orai1-R91W/Orai1-WT). Ca^{2+} stores were released with 2.5 μM ionomycin (*iono*) in Ca^{2+}-free medium followed by 1 mM Ca^{2+} (*arrows*). *Traces* (means ± S.E.) are the results for all cells in three independent experiments. *F,* summary scatter plots of peak Ca^{2+} entry normalized to Ca^{2+} entry with WT dimer (OO); results are means ± S.E. for all cells in three independent experiments represented by *E*. *G* and *H,* Ca^{2+} add-back measurements using fura-2-loaded HEK-O1^{ko}S1^{+} cells expressing similar levels of the C-terminal tdT-tagged Orai1-K85E homodimers (EE) or the K85E heterodimers (OE and EO). Ca^{2+} stores were released with 2.5 μM ionomycin in Ca^{2+}-free medium followed by 1 mM Ca^{2+} (*arrows*). *Traces* (means ± S.E.) are representative of all cells in three independent experiments. *I,* summary scatter plots of peak Ca^{2+} entry normalized to WT (OO) dimer Ca^{2+} entry; results are means ± S.E. of three independent experiments represented in *G* and *H*. *J* and *K,* representative *I/V* relationship of Ca^{2+} currents after store depletion in HEK-O1^{ko}S1^{+} cells transiently expressing OE (*J*) or EO (*K*). *L,* scatter plots of E-FRET between stably expressed STIM1-YFP and transiently expressed C-terminally CFP-tagged Orai1 dimers (OO, OE, EO, or EE, respectively) in HEK-O1^{ko}S1^{+} cells. E-FRET was measured at 5 min after addition of 2.5 μM ionomycin to deplete stores. **, $p < 0.001$. Results are means ± S.E. of three independent experiments.

Although the OE and EO heterodimers have reduced current, the pore properties have not changed. The effects on STIM1 binding of mutating the Lys-85 sites in the dimer support a model of close coupling between the M1-ext and the M4-ext, as suggested earlier (41). These two domains exist in a closely associated complex together with the 16-amino acid 2–3 loop joining the M2 and M3 helices (see Fig. 1*C*). Recent evidence indicates that the 2–3 loop mediates important communication with the M1-ext helix (43). Although the C-terminal M4-ext is the primary site for STIM1 binding to gate the channel, we would speculate that the entire cytosolic domain (M1-ext, 2–3 loop, and M4-ext) exists as a conformationally coupled entity, the alteration of which affects both STIM1 binding and gating of the channel. However, even though K85E alters STIM1 binding, we do not consider that the N terminus is a STIM1-binding site required for gating. Thus, we revealed earlier that a C-ter-

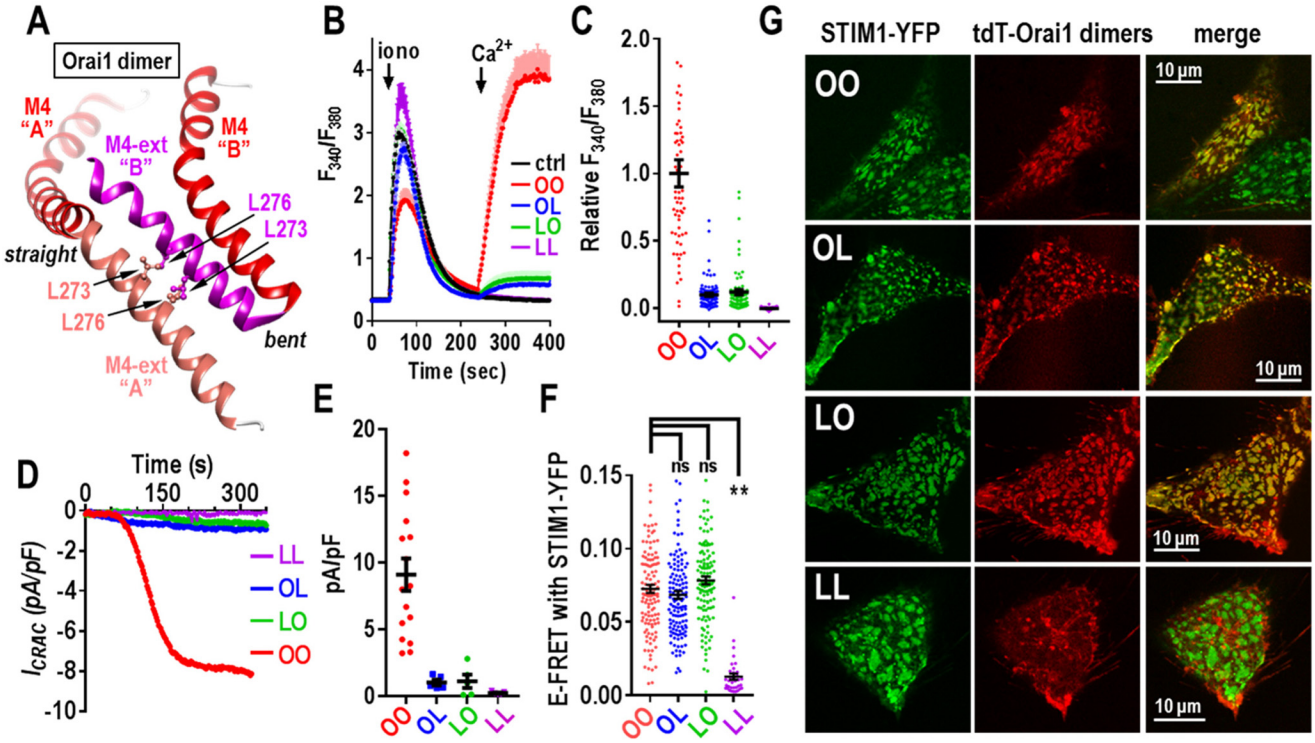

Figure 7. Effects of mutating the key STIM1-binding residue (Leu-273) of the Orai1 C terminus in concatenated Orai1 dimers. *A,* structural model Orai1 based on the dOrai M4 and M4 extensions (*M4-ext*), showing their configuration and interactions. The M4-ext from the straight monomer "*A*" and the M4-ext from the bent monomer "*B*" lie in a close antiparallel configuration stabilized by interactions between the Leu-273 and Leu-276 residues on each M4-ext. *B,* Ca^{2+} entry in fura-2–loaded HEK-O1^{ko}S1^{+} cells expressing similar levels of the C-terminal tdT-tagged Orai1 dimer constructs: OO (Orai1-WT/Orai1-WT), OL (Orai-WT/Orai1-L273D), LO (Orai1-L273D/Orai1-WT), LL (Orai1-L273D/Orai1-L273D), or untransfected control cells (*ctrl*). Ca^{2+} stores were released with 2.5 μM ionomycin (*iono*) in Ca^{2+}-free medium followed by addition of 1 mM Ca^{2+} (*arrows*). *Traces* (means ± S.E.) are representative of three independent experiments. *C,* summary scatter plots with means ± S.E. of peak Ca^{2+} entry normalized to peak Ca^{2+} entry for the OO dimer; all cells are shown from three independent experiments. *D,* whole-cell patch–clamp recording of HEK-O1^{ko}S1^{+} cells expressing OO, OL, LO, or LL, currents at −100 mV plotted against time. *E,* summary scatter plots of means ± S.E. of peak Ca^{2+} current density for all individual cells recorded for each of the Orai1 dimer constructs shown in *D*. *F,* scatter plots of E-FRET between stably expressed STIM1-YFP and transiently expressed C-terminally CFP-tagged Orai1 dimers (OO, OL, LO, or LL, respectively) in HEK-O1^{ko}S1^{+} cells. E-FRET was measured at 5 min after addition of 2.5 μM ionomycin to deplete stores. **, $p < 0.001$; *ns*, not significant. Results are means ± S.E. of three independent experiments. *G,* confocal images showing the localization of stably expressed STIM1-YFP and transiently-transfected Orai1-tdTdimers (OO, OL, LO, and LL) expressed in HEK-O1^{ko}S1^{+} cells. Images were taken 5 min after 2.5 μM ionomycin treatment to empty stores. In each case, confocal images show STIM1 and Orai1 dimers localized only in the PM layer immediately adjacent to the coverslip. For OO (*top row*), there are two cells; the centered cell expresses both STIM1-YFP and OO-tdT, and the lower right cell expresses only STIM1-YFP. Note: there is near-perfect co-localization of STIM and with the OO, OL, and LO Orai1 dimers; in contrast, there is no co-localization of STIM1 with the LL Orai1 dimer.

minal mutation in Orai1 that mimics STIM1-induced channel activation without any STIM1 present is similarly sensitive to the K85E mutation (13).

Probing the STIM1-Orai1 coupling interface at the C terminus of Orai1

We shifted our exploration of the function of Orai1 dimers to understanding more about the C-terminal M4-ext helix, the site at which STIM1 binds strongly and initiates activation of the channel. Unlike the N terminus, which has six identical helices, the dOrai crystal structure shows that the short 45-amino acid C-terminal M4-ext exists in two different configurations (Fig. 1, *A* and *C*). Thus, each dimer of Orai contains one M4-ext that is in an extended conformation, and one that is in a bent conformation (17). Based on the dOrai structure, the two M4-ext helices in Orai1 are likely attached in an antiparallel configuration through inter-helical hydrophobic interactions between the Leu-273 and Leu-276 residues in each helix (see Fig. 7*A*). Mutation of Leu-273 in Orai1 to either Asp or Ser is known to abolish binding of STIM1 and any store-dependent activation of the channel (27, 38, 41, 44–46). This likely stems from disruption of the two bound M4-ext helices, although how STIM associates with these helices is still unclear (47, 48). We constructed tdTomato-tagged Orai1 dimers in which either one or both monomers contained the L273D mutation. We tested the function of these dimers in HEK-O1^{ko}S1^{+} cells. As expected, the L273D mutant Orai1 homodimer (LL) gave no store-operated Ca^{2+} entry (Fig. 7, *B* and *C*) nor any current through the channel (Fig. 7, *D* and *E*). In contrast, the two Orai1 heterodimers (OL and LO) both gave a very small Ca^{2+} entry (Fig. 7, *B* and *C*). Current measurements also revealed that the conductance of the OL and LO heterodimers was extremely low (Fig. 7, *D* and *E*). Summary data for both the Ca^{2+} and current measurements reveal that the OL and LO heterodimers have less than 10% of the activity of the WT OO homodimer (Fig. 7, *C* and *E*).

We considered that the drastically decreased function of the OL and LO heterodimer channels might reflect a loss of the ability to bind STIM1. To address this question, we undertook FRET studies using another set of Orai1 dimers (OO, OL, LO, and LL) with C-terminal CFP tags. These were transiently expressed in cells stably expressing STIM1-YFP. Surprisingly,

we observed that the Orai1 OL and LO heterodimers did not have a defect in STIM1-binding activity. Thus, after store depletion, the FRET values for OO, OL, and LO with STIM1-YFP were not significantly different (Fig. 7*F*). As expected, the FRET value for the LL homodimer was much decreased indicating that STIM1 binding was effectively abolished. In further experiments, we undertook direct visualization of cells co-expressing Orai-tdT dimers and STIM1-YFP (Fig. 7*G*). In these studies we utilized HEK-O1^{ko}S1^{+} cells and transiently transfected each of the Orai1-tdT–tagged dimers. The results are highly consistent with the FRET studies. In cells transfected with the WT Orai1-OO homodimer (Fig. 7*G*, *top row, upper left cell*), there was almost complete co-localization of OO-tdT with STIM1-YFP. The two molecules co-localized within the same clearly observable punctal regions in cells that represent the ER–PM junctional areas. An almost identical pattern of co-localization was also seen in cells expressing the OL and LO heterodimers (Fig. 7*G*, *2nd* and *3rd rows*). These results contrast dramatically with cells expressing the LL mutant homodimer (Fig. 7*G*, *bottom row*). In this case, there is clearly no co-localization of the LL dimer with the STIM1 protein at the PM junctions, even though STIM1 can still form puncta by interacting with PM phospholipids in the ER–PM junctions (49, 50). Indeed, as seen in Fig. 7*G* (*top row*), the lower right cell did not express Orai1, yet the STIM1 still entered puncta exactly the same as in the cell co-expressing Orai1.

These results provide important new information about the critical nature of the Orai1 C-terminal configuration in mediating gating of the Orai1 channel. The single L273D mutation in the OL or LO Orai1 heterodimers drastically impedes the ability of Orai1 to be gated by STIM1; however, the same heterodimers have not lost any significant ability to bind STIM1. Recent studies indicate that binding of STIM1 to the Orai1 C-terminal M4-ext is sufficient to gate the channel (13). This interaction causes an allosteric change in the Orai1 channel that is propagated from the M4-ext through the M3, M2, and M1 helices resulting in certain pore-lining M1 residues undergoing a structural alteration that constitutes gating of the channel (13, 51). From the LL-Orai1 homodimer result, the two M4-ext helices have likely undergone unfolding sufficient to completely prevent STIM1 binding. With the single L273D mutation in the OL or LO heterodimers, the rearrangement must be much more subtle such that STIM1 binding is largely intact. Yet, the propagation of allosteric change across the protein to gate the channel is almost completely lost. Thus, it seems that the M4-ext may undergo only a small conformational change to initiate gating. This conclusion agrees with studies on cross-linking of the M4-ext helices by Tirado-Lee *et al.* (27). Recent structural analysis has suggested that the interacting pairs of M4-ext helices act as latches on the outside of the channel that must be opened to allow the M1-ext helices to expand outward thus permitting the cytosolic mouth of the pore to open (36). This model was based on a crystallized dOrai structure that stabilized the unlatched channel with straightened M4-ext helices. However, this dOrai configuration was not based on any input from STIM proteins. Our results indicate that the initial STIM1-induced alteration of the M4-ext helices is extremely subtle and unlikely to be a large unlatching of the entire Orai outer structure.

Concluding remarks

The use of concatenated Orai1 dimers has proven highly useful in determining the role of key residues in the channel pore and the STIM1-binding site of Orai1. Using a CRISPR/Cas9-derived Orai1-free background cell system, the dimer concatemers are reliable probes for the function of the hexameric Orai1 channel. Two highlights of these findings are particularly prominent. First, our studies provide some important new understanding on the properties of the pore-selectivity filter that normally functions with six charged Glu residues. We speculate that these residues may have sufficient flexibility to allow formation of two Ca^{2+}-binding sites within the selectivity filter, as suggested recently (36). The symmetrical and somewhat conservative replacement of three Glu residues with three intervening Gln residues (formed with OQ or QO dimers) may prevent formation of the putative second site and render the pore as a nonselective cation channel. Functionally, this construct operates the same as six Asp residues in the selectivity filter; however, in that case the shortened headgroups lack the dimension and flexibility to form two sites. Future structure and modeling studies might examine this possibility. Second, our studies also throw new light on the Orai1 C-terminal binding site for STIM1. The OL and LO Orai1 heterodimers appear to have little change in their STIM1-binding properties, yet they have almost entirely lost the ability to mediate gating of the channel. This result emphasizes the exquisitely precise nature of the initial interacting site for STIM1 on Orai1 (the M4-ext) through which it induces channel activation. The two M4-ext sites likely propagate this allosteric gating of the channel across the tightly packed M3, M2, and M1 helices as suggested recently (13).

Experimental procedures

DNA constructs

Concatenated Orai1 dimers were constructed as described earlier. The 36-amino acid linker sequence is TSSSTMLHPGLSPGLLPLHPASIGGSGGSGGSGRAT (25). For Orai1 heterodimers, point mutations in the M1 or M4-ext helices (Glu-106, Val-102, Arg-91, Lys-85, and Leu-273) were performed on Orai1-WT monomers using the QuikChange Lightning Site-directed Mutagenesis kit (Agilent; 210518) and then inserted into the ptdTomato–N1–Orai1 plasmid with XhoI and BamHI restriction sites. For C-terminal CFP-tagged constructs, the tdT tag was changed to ECFP with BamHI and NotI restriction sites.

Cell culture and transfection

HEK-O1^{ko} cells and the HEK-O1^{ko}S1^{+} cell line were generated using the CRISPR-Cas9 nickase system as described earlier (25). Cells were cultured in Dulbecco's modified Eagle's medium (Corning Cellgro) supplemented with 10% fetal bovine serum, penicillin, and streptomycin (Gemini Bioproducts, CA) containing puromycin (2 μg/ml) at 37 °C with 5% CO_2. All transfections were performed by electroporation at 180 V, 25

ms in 4-mm cuvettes (Molecular Bio-Products) using the Bio-Rad Gene Pulser Xcell system in Opti-MEM medium, as described previously (52). Experiments were all performed 18–24 h after transfection.

Cytosolic Ca^{2+} measurements

Cytosolic Ca^{2+} levels were measured as described earlier (53) by ratiometric imaging using fura-2 (Molecular Probes). Cells were used 18–24 h after transfection and incubated with 2 μM fura-2 in buffer containing 107 mM NaCl, 7.2 mM KCl, 1.2 mM $MgCl_2$, 1 mM $CaCl_2$, 11.5 mM glucose, 0.1% BSA, 20 mM HEPES (pH 7.2), for 30 min at room temperature, followed by treatment with fura-2 free solution for another 30 min. Fluorescence ratio imaging was measured utilizing the Leica DMI 6000B fluorescence microscope and Hamamatsu camera ORCA-Flash 4 controlled by Slidebook 6.0 software (Intelligent Imaging Innovations; Denver, CO) as described previously (54). Consecutive excitation at 340 nm (F_{340}) and 380 nm (F_{380}) was undertaken every 2 s, and emission fluorescence was collected at 505 nm. Intracellular Ca^{2+} levels are shown as F_{340}/F_{380} ratios obtained from groups of 8–25 single cells on coverslips. For the Orai1 concatemer experiments, data are shown for cells expressing a narrow range of tdTomato fluorescence to maximize consistency of responses between cells. For each concatemer experiment, we simultaneously examined each set of mutants with the corresponding WT concatemer. The expression levels for WT and mutant concatemers were within a similar narrow range of fluorescence intensity. All Ca^{2+} imaging experiments were performed at room temperature, and representative traces of at least three independent repeats are shown. Scatter plots with means ± S.E. are shown for all the cells recorded.

Deconvolved fluorescence image analysis

For imaging of cells, we used the inverted Leica DMI 6000B automated fluorescence microscope and Hamamatsu ORCA-Flash 4 camera controlled by Slidebook software to collect and analyze high-resolution fluorescence images. For the PM localization studies of tdTomato-tagged Orai1 concatemers, stacks of 10–20 3D z axis image-planes close to the cell-glass interface were collected at 0.35-μm steps. The no-neighbor deconvolution function of the Slidebook 6.0 software was used to analyze images and to derive enhanced deconvolved images with minimized fluorescence contamination from out-of-focus planes. The tdT-tagged Orai1 concatemer images shown were typical of at least three independent analyses.

Confocal imaging

Cells transfected with tdT-tagged constructs were imaged 14–20 h after transfection. Live cell images were collected on the inverted Leica TCS SP8 confocal microscope using a ×63/1.40 oil objective. Images shown are typical of at least three independent experiments.

Electrophysiological measurements and pore size estimation

Whole-cell patch–clamp recording was performed on HEK-$O1^{ko}S1^{+}$ cells transiently transfected with tdT-tagged Orai1 concatemer constructs, or not transfected, as described (11). To passively deplete ER Ca^{2+} stores, the pipette solution contained 135 mM cesium aspartate, 10 mM HEPES, 8 mM $MgCl_2$, and 20 mM BAPTA (pH 7.2 with CsOH). For measuring constitutively active currents, HEK-$O1^{ko}$ cells were transiently transfected with different Orai1-V102C concatemers, and the pipette solution included 135 mM cesium-aspartate, 10 mM HEPES, 5 mM $MgCl_2$, 10 mM EGTA, and 3 mM $CaCl_2$. The bath solution contained 130 mM NaCl, 4.5 mM KCl, 5 mM HEPES, 10 mM dextrose, 10 mM TEA-Cl, and 20 mM $CaCl_2$ (pH 7.2 with NaOH). Divalent free solution included 150 mM NaCl, 5 mM HEPES, 10 mM TEA-Cl, 10 mM HEDTA, and 1 mM EDTA (pH 7.4). When indicated, 150 mM NaCl was substituted by 150 mM methylamine-HCl, dimethylamine-HCl, trimethylamine-HCl, or tetramethylamine-HCl. I_{CRAC} was recorded until steady state, and then the external solution was switched to the different methylammonium-DVF solutions indicated. Currents were recorded in the standard whole-cell configuration using the EPC-10 amplifier (HEKA). Glass electrodes with a typical resistance of 2–4 megohms were pulled using a P-97 pipette puller (Sutter Instruments). A 50-ms step to −100 mV from a holding potential of 0 mV, followed by a 50-ms ramp from −100 to 100 mV, was delivered every 2 s. Currents were filtered at 3.0 kHz and sampled at 20 kHz. A +10-mV junction potential compensation was applied to correct the liquid junction potential between the bath and pipette solutions. The current measure at −100 mV was used in I–V curves. All data were acquired with Patch Master and analyzed using FitMaster and Graph Pad Prism 6.

Using the Goldman-Hodgkin-Katz voltage Equation 1, relative permeabilities of the different methylated ammonium ions and Na^+ (P_x/P_{Na}) were calculated from changes in the reversal potential,

$$P_x/P_{Na} = \frac{[Na]_0}{[X]_0} e^{\Delta E_{rev} F/RT} \quad \text{(Eq. 1)}$$

in which $[X]_0$ and $[Na]_0$ are the external ionic concentrations; ΔE_{rev} is the change in reversal potential when switched to the testing cation; R is the universal gas constant; T is the temperature in Kelvin; and F is Faraday's constant.

We estimated pore dimensions using the relative ion permeability ratios, as described earlier (35), assuming that ion permeability is limited mainly by steric hindrance. The relative permeability was calculate from Equation 2,

$$\frac{P_x}{P_{Na}} = k\left(1 - \frac{d_{ion}}{d_{pore}}\right)^2 \quad \text{(Eq. 2)}$$

in which k is a proportionality constant; d_{ion} is the ion diameter, and d_{pore} is the pore diameter (55, 56). An estimate for d_{pore} was derived by relating decrease in permeability ratio to the increase in organic cation size.

Western blotting analyses

Cells were washed with ice-cold PBS and lysed on ice using lysis buffer (RIPA, Sigma, and 1× protease inhibitor mixture) for 30 min, followed by centrifugation at 14,000 × g for 10 min at 4 °C. Supernatants were collected, and protein was quantified using Bio-Rad DC kits. Proteins were resolved on 4–15% NuPAGE BisTris precast gels and transferred to Bio-Rad

Immuno-Blot polyvinylidene difluoride membranes. After blocking in 5% nonfat milk for 1 h at room temperature, the membrane was incubated with primary antibody at 4 °C overnight. Membranes were washed three times in PBST and incubated with secondary antibody for 1 h at room temperature. Subsequently, membranes were washed three times with PBST. Peroxidase activity was examined with Pierce ECL Plus Western blotting substrate (ThermoFisher Scientific), and fluorescence was collected using the FluorChem M imager (ProteinSimple).

Förster resonance energy transfer measurements

To determine FRET signals between stably expressed STIM1-YFP and transiently expressed CFP-tagged Orai1 dimers, we used the Leica DMI 6000B inverted automated fluorescence microscope equipped with CFP (excitation 438/emission 483), YFP (excitation 500/emission 542), and FRET (excitation 438/emission 542) filter cubes. At each time point, three sets of images (CFP, YFP, and FRET) were collected at room temperature using a ×40 oil objective (numerical aperture 1.35; Leica) and processed using Slidebook 6.0 software (Intelligent Imaging Innovations). Images were captured at 20-s intervals. Exposure times for the CFP, YFP, and FRET channels were 1000, 250, and 1000 ms, respectively. The decreased YFP channel exposure time compensates for the greater fluorescence intensity of YFP compared with CFP. Three-channel–corrected FRET was calculated using Equation 3,

$$F_c = I_{DA} - F_d/D_d \times I_{DD} - Fa/Da \times I_{AA} \quad \text{(Eq. 3)}$$

where I_{DD}, $I_{AA,}$ and I_{DA} represent the background-subtracted CFP, YFP, and FRET images, respectively; F_c represents the corrected energy transfer; F_d/D_d represents measured bleed-through of CFP through the FRET filter (0.457) and Fa/Da is the bleed-through of YFP through the FRET filter (0.19). We used the E-FRET method to analyze three-cube FRET images as describe by Ref. 57 using Equation 4,

$$E_{app} = F_c/(F_c + G \times I_{DD}) \quad \text{(Eq. 4)}$$

in which G is the instrument-specific constant (44, 57). The EYFP-ECFP construct, made as described above, was used to determine the G-parameter for E-FRET calculations. The value of G was determined by measuring the CFP fluorescence increase after YFP acceptor photobleaching using HEK-WT cells transiently transfected with the pEYFP-ECFP construct. The value of G was calculated as 1.9 ± 0.1 (n = 32 cells). For studies determining E-FRET between YFP and CFP constructs, cells with a narrow range of YFP/CFP ratios were selected to ensure comparability between measurements. In all our E-FRET summary data, a region close to the PM was selected, and E-FRET analysis was conducted on cells with similar YFP/CFP ratios.

Author contributions—X. C., R. M. N., J. H. B., M. T., Y. Z., and D. L. G. conceptualization; X. C. data curation; X. C., R. M. N., and D. L. G. formal analysis; X. C., R. M. N., N. A. L., and R. A. investigation; X. C. and D. L. G. methodology; X. C. and D. L. G. writing-original draft; X. C., N. A. L., R. A., Y. W., M. T., Y. Z., and D. L. G. writing-review and editing; R. M. N. and D. L. G. funding acquisition; D. L. G. supervision.

References

1. Prakriya, M., and Lewis, R. S. (2015) Store-operated calcium channels. *Physiol. Rev.* **95,** 1383–1436 CrossRef Medline
2. Amcheslavsky, A., Wood, M. L., Yeromin, A. V., Parker, I., Freites, J. A., Tobias, D. J., and Cahalan, M. D. (2015) Molecular biophysics of Orai store-operated Ca channels. *Biophys. J.* **108,** 237–246 CrossRef Medline
3. Shim, A. H., Tirado-Lee, L., and Prakriya, M. (2015) Structural and functional mechanisms of CRAC channel regulation. *J. Mol. Biol.* **427,** 77–93 CrossRef Medline
4. Zhou, Y., Cai, X., Nwokonko, R. M., Loktionova, N. A., Wang, Y., and Gill, D. L. (2017) The STIM-Orai coupling interface and gating of the Orai1 channel. *Cell Calcium* **63,** 8–13 CrossRef Medline
5. Soboloff, J., Rothberg, B. S., Madesh, M., and Gill, D. L. (2012) STIM proteins: dynamic calcium signal transducers. *Nat. Rev. Mol. Cell Biol.* **13,** 549–565 CrossRef Medline
6. Hogan, P. G. (2015) The STIM1-ORAI1 microdomain. *Cell Calcium* **58,** 357–367 CrossRef Medline
7. Derler, I., Jardin, I., and Romanin, C. (2016) Molecular mechanisms of STIM/Orai communication. *Am. J. Physiol. Cell Physiol.* **310,** C643–C662 CrossRef Medline
8. Kar, P., and Parekh, A. (2013) STIM proteins, Orai1 and gene expression. *Channels* **7,** 374–378 CrossRef Medline
9. Zhou, Y., Trebak, M., and Gill, D. L. (2015) Calcium signals tune the fidelity of transcriptional responses. *Mol. Cell* **58,** 197–199 CrossRef Medline
10. Feske, S., Wulff, H., and Skolnik, E. Y. (2015) Ion channels in innate and adaptive immunity. *Annu. Rev. Immunol.* **33,** 291–353 CrossRef Medline
11. Wang, X., Wang, Y., Zhou, Y., Hendron, E., Mancarella, S., Andrake, M. D., Rothberg, B. S., Soboloff, J., and Gill, D. L. (2014) Distinct Orai-coupling domains in STIM1 and STIM2 define the Orai-activating site. *Nat. Commun.* **5,** 3183 CrossRef Medline
12. Zhou, Y., Wang, X., Wang, X., Loktionova, N. A., Cai, X., Nwokonko, R. M., Vrana, E., Wang, Y., Rothberg, B. S., and Gill, D. L. (2015) STIM1 dimers undergo unimolecular coupling to activate Orai1 channels. *Nat. Commun.* **6,** 8395 CrossRef Medline
13. Zhou, Y., Cai, X., Loktionova, N. A., Wang, X., Nwokonko, R. M., Wang, X., Wang, Y., Rothberg, B. S., Trebak, M., and Gill, D. L. (2016) The STIM1-binding site nexus remotely controls Orai1 channel gating. *Nat. Commun.* **7,** 13725 CrossRef Medline
14. Zhou, Y., Nwokonko, R. M., Cai, X., Loktionova, N. A., Abdulqadir, R., Xin, P., Niemeyer, B. A., Wang, Y., Trebak, M., and Gill, D. L. (2018) Cross-linking of Orai1 channels by STIM proteins. *Proc. Natl. Acad. Sci. U.S.A.* **115,** E3398–E3407 CrossRef Medline
15. Rothberg, B. S., Wang, Y., and Gill, D. L. (2013) Orai channel pore properties and gating by STIM: implications from the Orai crystal structure. *Sci. Signal.* **6,** pe9 Medline
16. Derler, I., Jardin, I., and Romanin, C. (2016) Molecular mechanisms of STIM/Orai communication. *Am. J. Physiol. Cell Physiol.* **310,** C643–C662 CrossRef Medline
17. Hou, X., Pedi, L., Diver, M. M., and Long, S. B. (2012) Crystal structure of the calcium release-activated calcium channel Orai. *Science* **338,** 1308–1313 CrossRef Medline
18. Penna, A., Demuro, A., Yeromin, A. V., Zhang, S. L., Safrina, O., Parker, I., and Cahalan, M. D. (2008) The CRAC channel consists of a tetramer formed by Stim-induced dimerization of Orai dimers. *Nature* **456,** 116–120 CrossRef Medline
19. Mignen, O., Thompson, J. L., and Shuttleworth, T. J. (2008) Orai1 subunit stoichiometry of the mammalian CRAC channel pore. *J. Physiol.* **586,** 419–425 CrossRef Medline
20. Ji, W., Xu, P., Li, Z., Lu, J., Liu, L., Zhan, Y., Chen, Y., Hille, B., Xu, T., and Chen, L. (2008) Functional stoichiometry of the unitary calcium-release-activated calcium channel. *Proc. Natl. Acad. Sci. U.S.A.* **105,** 13668–13673 CrossRef Medline
21. Maruyama, Y., Ogura, T., Mio, K., Kato, K., Kaneko, T., Kiyonaka, S., Mori, Y., and Sato, C. (2009) Tetrameric Orai1 is a teardrop-shaped molecule with a long, tapered cytoplasmic domain. *J. Biol. Chem.* **284,** 13676–13685 CrossRef Medline

22. Madl, J., Weghuber, J., Fritsch, R., Derler, I., Fahrner, M., Frischauf, I., Lackner, B., Romanin, C., and Schütz, G. J. (2010) Resting state Orai1 diffuses as homotetramer in the plasma membrane of live mammalian cells. *J. Biol. Chem.* **285,** 41135–41142 CrossRef Medline
23. Demuro, A., Penna, A., Safrina, O., Yeromin, A. V., Amcheslavsky, A., Cahalan, M. D., and Parker, I. (2011) Subunit stoichiometry of human Orai1 and Orai3 channels in closed and open states. *Proc. Natl. Acad. Sci. U.S.A.* **108,** 17832–17837 CrossRef Medline
24. Thompson, J. L., and Shuttleworth, T. J. (2013) How many Orai's does it take to make a CRAC channel? *Sci. Rep.* **3,** 1961 CrossRef Medline
25. Cai, X., Zhou, Y., Nwokonko, R. M., Loktionova, N. A., Wang, X., Xin, P., Trebak, M., Wang, Y., and Gill, D. L. (2016) The Orai1 store-operated calcium channel functions as a hexamer. *J. Biol. Chem.* **291,** 25764–25775 CrossRef Medline
26. Yen, M., Lokteva, L. A., and Lewis, R. S. (2016) Functional analysis of Orai1 concatemers supports a hexameric stoichiometry for the CRAC channel. *Biophys. J.* **111,** 1897–1907 CrossRef Medline
27. Tirado-Lee, L., Yamashita, M., and Prakriya, M. (2015) Conformational changes in the Orai1 C terminus evoked by STIM1 binding. *PLoS ONE* **10,** e0128622 CrossRef Medline
28. Feske, S., Gwack, Y., Prakriya, M., Srikanth, S., Puppel, S. H., Tanasa, B., Hogan, P. G., Lewis, R. S., Daly, M., and Rao, A. (2006) A mutation in Orai1 causes immune deficiency by abrogating CRAC channel function. *Nature* **441,** 179–185 CrossRef Medline
29. Vig, M., Beck, A., Billingsley, J. M., Lis, A., Parvez, S., Peinelt, C., Koomoa, D. L., Soboloff, J., Gill, D. L., Fleig, A., Kinet, J. P., and Penner, R. (2006) CRACM1 multimers form the ion-selective pore of the CRAC channel. *Curr. Biol.* **16,** 2073–2079 CrossRef Medline
30. Yeromin, A. V., Zhang, S. L., Jiang, W., Yu, Y., Safrina, O., and Cahalan, M. D. (2006) Molecular identification of the CRAC channel by altered ion selectivity in a mutant of Orai. *Nature* **443,** 226–229 CrossRef Medline
31. Gwack, Y., Srikanth, S., Feske, S., Cruz-Guilloty, F., Oh-hora, M., Neems, D. S., Hogan, P. G., and Rao, A. (2007) Biochemical and functional characterization of Orai family proteins. *J. Biol. Chem.* **282,** 16232–16243 CrossRef Medline
32. Lis, A., Peinelt, C., Beck, A., Parvez, S., Monteilh-Zoller, M., Fleig, A., and Penner, R. (2007) CRACM1, CRACM2, and CRACM3 are store-operated Ca^{2+} channels with distinct functional properties. *Curr. Biol.* **17,** 794–800 CrossRef Medline
33. Wei-Lapierre, L., Carrell, E. M., Boncompagni, S., Protasi, F., and Dirksen, R. T. (2013) Orai1-dependent calcium entry promotes skeletal muscle growth and limits fatigue. *Nat. Commun.* **4,** 2805 CrossRef Medline
34. Yamashita, M., Navarro-Borelly, L., McNally, B. A., and Prakriya, M. (2007) Orai1 mutations alter ion permeation and Ca^{2+}-dependent fast inactivation of CRAC channels: evidence for coupling of permeation and gating. *J. Gen. Physiol.* **130,** 525–540 CrossRef Medline
35. Prakriya, M., and Lewis, R. S. (2006) Regulation of CRAC channel activity by recruitment of silent channels to a high open-probability gating mode. *J. Gen. Physiol.* **128,** 373–386 CrossRef Medline
36. Hou, X., Burstein, S. R., and Long, S. B. (2018) Structures reveal opening of the store-operated calcium channel Orai. *bioRxiv* 284034 CrossRef
37. McNally, B. A., Somasundaram, A., Yamashita, M., and Prakriya, M. (2012) Gated regulation of CRAC channel ion selectivity by STIM1. *Nature* **482,** 241–245 CrossRef Medline
38. Muik, M., Frischauf, I., Derler, I., Fahrner, M., Bergsmann, J., Eder, P., Schindl, R., Hesch, C., Polzinger, B., Fritsch, R., Kahr, H., Madl, J., Gruber, H., Groschner, K., and Romanin, C. (2008) Dynamic coupling of the putative coiled-coil domain of ORAI1 with STIM1 mediates ORAI1 channel activation. *J. Biol. Chem.* **283,** 8014–8022 CrossRef Medline
39. Thompson, J. L., Mignen, O., and Shuttleworth, T. J. (2009) The Orai1 severe combined immune deficiency mutation and calcium release-activated Ca^{2+} channel function in the heterozygous condition. *J. Biol. Chem.* **284,** 6620–6626 CrossRef Medline
40. Lis, A., Zierler, S., Peinelt, C., Fleig, A., and Penner, R. (2010) A single lysine in the N-terminal region of store-operated channels is critical for STIM1-mediated gating. *J. Gen. Physiol.* **136,** 673–686 CrossRef Medline
41. McNally, B. A., Somasundaram, A., Jairaman, A., Yamashita, M., and Prakriya, M. (2013) The C- and N-terminal STIM1 binding sites on Orai1 are required for both trapping and gating CRAC channels. *J. Physiol.* **591,** 2833–2850 CrossRef Medline
42. Gudlur, A., Quintana, A., Zhou, Y., Hirve, N., Mahapatra, S., and Hogan, P. G. (2014) STIM1 triggers a gating rearrangement at the extracellular mouth of the ORAI1 channel. *Nat. Commun.* **5,** 5164 CrossRef Medline
43. Fahrner, M., Pandey, S. K., Muik, M., Traxler, L., Butorac, C., Stadlbauer, M., Zayats, V., Krizova, A., Plenk, P., Frischauf, I., Schindl, R., Gruber, H. J., Hinterdorfer, P., Ettrich, R., Romanin, C., and Derler, I. (2018) Communication between N terminus and loop2 tunes Orai activation. *J. Biol. Chem.* **293,** 1271–1285 CrossRef Medline
44. Navarro-Borelly, L., Somasundaram, A., Yamashita, M., Ren, D., Miller, R. J., and Prakriya, M. (2008) STIM1-ORAI1 interactions and ORAI1 conformational changes revealed by live-cell FRET microscopy. *J. Physiol.* **586,** 5383–5401 CrossRef Medline
45. Frischauf, I., Muik, M., Derler, I., Bergsmann, J., Fahrner, M., Schindl, R., Groschner, K., and Romanin, C. (2009) Molecular determinants of the coupling between STIM1 and Orai channels: differential activation of Orai1–3 channels by a STIM1 coiled-coil mutant. *J. Biol. Chem.* **284,** 21696–21706 CrossRef Medline
46. Li, Z., Liu, L., Deng, Y., Ji, W., Du, W., Xu, P., Chen, L., and Xu, T. (2011) Graded activation of CRAC channel by binding of different numbers of STIM1 to Orai1 subunits. *Cell Res.* **21,** 305–315 CrossRef Medline
47. Stathopulos, P. B., Schindl, R., Fahrner, M., Zheng, L., Gasmi-Seabrook, G. M., Muik, M., Romanin, C., and Ikura, M. (2013) STIM1/Orai1 coiled-coil interplay in the regulation of store-operated calcium entry. *Nat. Commun.* **4,** 2963 CrossRef Medline
48. Maus, M., Jairaman, A., Stathopulos, P. B., Muik, M., Fahrner, M., Weidinger, C., Benson, M., Fuchs, S., Ehl, S., Romanin, C., Ikura, M., Prakriya, M., and Feske, S. (2015) Missense mutation in immunodeficient patients shows the multifunctional roles of coiled-coil domain 3 (CC3) in STIM1 activation. *Proc. Natl. Acad. Sci. U.S.A.* **112,** 6206–6211 CrossRef Medline
49. Liou, J., Fivaz, M., Inoue, T., and Meyer, T. (2007) Live-cell imaging reveals sequential oligomerization and local plasma membrane targeting of stromal interaction molecule 1 after Ca^{2+} store depletion. *Proc. Natl. Acad. Sci. U.S.A.* **104,** 9301–9306 CrossRef Medline
50. Park, C. Y., Hoover, P. J., Mullins, F. M., Bachhawat, P., Covington, E. D., Raunser, S., Walz, T., Garcia, K. C., Dolmetsch, R. E., and Lewis, R. S. (2009) STIM1 clusters and activates CRAC channels via direct binding of a cytosolic domain to Orai1. *Cell* **136,** 876–890 CrossRef Medline
51. Palty, R., Fu, Z., and Isacoff, E. Y. (2017) Sequential steps of CRAC channel activation. *Cell Rep.* **19,** 1929–1939 CrossRef Medline
52. Mancarella, S., Wang, Y., and Gill, D. L. (2011) Signal transduction: STIM1 senses both Ca^{2+} and heat. *Nat. Chem. Biol.* **7,** 344–345 CrossRef Medline
53. Soboloff, J., Spassova, M. A., Hewavitharana, T., He, L. P., Xu, W., Johnstone, L. S., Dziadek, M. A., and Gill, D. L. (2006) STIM2 is an inhibitor of STIM1-mediated store-operated Ca^{2+} entry. *Curr. Biol.* **16,** 1465–1470 CrossRef Medline
54. Mancarella, S., Wang, Y., Deng, X., Landesberg, G., Scalia, R., Panettieri, R. A., Mallilankaraman, K., Tang, X. D., Madesh, M., and Gill, D. L. (2011) Hypoxia-induced acidosis uncouples the STIM-Orai calcium signaling complex. *J. Biol. Chem.* **286,** 44788–44798 CrossRef Medline
55. Dwyer, T. M., Adams, D. J., and Hille, B. (1980) The permeability of the endplate channel to organic cations in frog muscle. *J. Gen. Physiol.* **75,** 469–492 CrossRef Medline
56. Burnashev, N., Villarroel, A., and Sakmann, B. (1996) Dimensions and ion selectivity of recombinant AMPA and kainate receptor channels and their dependence on Q/R site residues. *J. Physiol.* **496,** 165–173 CrossRef Medline
57. Zal, T., and Gascoigne, N. R. (2004) Photobleaching-corrected FRET efficiency imaging of live cells. *Biophys. J.* **86,** 3923–3939 CrossRef Medline